

This is a self-archived version of an original article. This version may differ from the original in pagination and typographic details.

Author(s): Modi, Vaibhav; Donnini, Serena; Groenhof, Gerrit; Morozov, Dmitry

Title: Protonation of the Biliverdin IX α Chromophore in the Red and Far-Red Photoactive States of Bacteriophytochrome

Year: 2019

Version: Accepted version (Final draft)

Copyright: © 2019 American Chemical Society.

Rights: In Copyright

Rights url: <http://rightsstatements.org/page/InC/1.0/?language=en>

Please cite the original version:

Modi, V., Donnini, S., Groenhof, G., & Morozov, D. (2019). Protonation of the Biliverdin IX α Chromophore in the Red and Far-Red Photoactive States of Bacteriophytochrome. *Journal of Physical Chemistry B*, 123(10), 2325-2334. <https://doi.org/10.1021/acs.jpcb.9b01117>

Protonation of the Biliverdin IX β Chromophore in the Red and Far-Red Photoactive States of Bacteriophytochrome

Vaibhav Modi, Serena Donnini, Gerrit Groenhof, and Dmitry Morozov

J. Phys. Chem. B, **Just Accepted Manuscript** • DOI: 10.1021/acs.jpcb.9b01117 • Publication Date (Web): 14 Feb 2019

Downloaded from <http://pubs.acs.org> on February 18, 2019

Just Accepted

"Just Accepted" manuscripts have been peer-reviewed and accepted for publication. They are posted online prior to technical editing, formatting for publication and author proofing. The American Chemical Society provides "Just Accepted" as a service to the research community to expedite the dissemination of scientific material as soon as possible after acceptance. "Just Accepted" manuscripts appear in full in PDF format accompanied by an HTML abstract. "Just Accepted" manuscripts have been fully peer reviewed, but should not be considered the official version of record. They are citable by the Digital Object Identifier (DOI®). "Just Accepted" is an optional service offered to authors. Therefore, the "Just Accepted" Web site may not include all articles that will be published in the journal. After a manuscript is technically edited and formatted, it will be removed from the "Just Accepted" Web site and published as an ASAP article. Note that technical editing may introduce minor changes to the manuscript text and/or graphics which could affect content, and all legal disclaimers and ethical guidelines that apply to the journal pertain. ACS cannot be held responsible for errors or consequences arising from the use of information contained in these "Just Accepted" manuscripts.



Protonation of the Biliverdin IX α Chromophore in the Red and Far-red Photoactive States of Bacteriophytochrome

Vaibhav Modi,¹ Serena Donnini,² Gerrit Groenhof,¹ Dmitry Morozov^{1*}

¹Department of Chemistry and NanoScience Center, University of Jyväskylä, P. O. Box 35, 40014 University of Jyväskylä, Jyväskylä, Finland

²Department of Biological and Environmental Science and NanoScience Center, University of Jyväskylä, P. O. Box 35, 40014 University of Jyväskylä, Jyväskylä, Finland.

KEYWORDS: Phytochrome, Molecular Dynamics, Quantum Chemistry, Excited States.

ABSTRACT: The tetra-pyrrole chromophore Biliverdin IX α (BV) in bacteriophytochrome from *Deinococcus radiodurans* (DrBphP) is usually assumed to be fully protonated, but this assumption has not been systematically validated by experiments or extensive computations. Here we use force field MD simulations and QM/MM calculations with DFT and XMCQDPT2 methods to investigate the effect of the five most probable protonation forms of BV on structural stability, binding pocket interactions and absorption spectra in the two photochromic states of DrBphP. While agreement with x-ray structural data and measured UV/vis spectra suggest that in both states the protonated form of the chromophore dominates, we also find that a minor

population with a deprotonated D-ring could contribute to the red-shifted tail in the absorption spectra.

Introduction

Light sensitive signaling cascades in various plants, fungi and bacteria are controlled by a photochemical mechanism involving photoactive proteins.^{1,2} Phytochromes belong to the class of photo-receptors that exist in nature with the ability to reversibly inter-convert on the time-scale of μ s-to-ms between two structurally distinct states: Pr-dark, and Pfr-illuminated. These states respond to red light (Pr) and far-red light (Pfr) and regulate numerous cellular functions, such as photo-morphogenesis, flowering, shade avoidance in plants, and pigment synthesis in bacteria^{3,4}. The red/far-red light family phytochromes exist as dimers. Upon red light (700 nm) absorption the Pr state undergoes large conformational changes to photo-convert via various intermediate states into the Pfr state. The reverse photo-conversion to Pr from Pfr state is initiated either by far-red light (750 nm) absorption or by dark thermal relaxation⁵. There are also bacterial phytochromes, for which the Pr-to-Pfr photo-conversion occurs in darkness^{6, 7}. These phytochromes with reversed dark thermal relaxation mechanism are termed as bathy phytochromes.

Recently, X-ray structures of the photo-sensory unit of phytochrome from *Deinococcus radiodurans* (DrBphP) have become available^{5,8,9}, which are of great help to make a beginning in understanding the molecular mechanism responsible for the photo-response of this protein. The structural unit of the core module consists of a PAS (Period, Aryl hydrocarbon receptor nuclear translocator, and Single-minded protein), GAF (cGMP-specific phosphodiesterase, adenylate cyclase, and Fhl proteins), and PHY (photochromic phytochrome) domain, while the full length

phytochrome has also a histidine kinase (HK) domain attached to the PHY domain at the C-terminal end. The phytochromes can be classified based on the type and site of the covalently bound tetra-pyrrole bilin chromophore that varies between organisms: phycocyanobilin (PΦB) in cyanobacterial phytochromes and phytochromobilin (PCB) in plant phytochromes have a covalent bond between their C3¹ atom (CBA atom in Figure 1a) and cysteine residue Cys259 in the GAF domain^{4,10,11}, while biliverdin IX α (BV) found in bacteriophytochromes is bound to the protein via C3² carbon atom (CBA atom in Figure 1a) to cysteine residue Cys24 in the PAS domain^{8,12}.

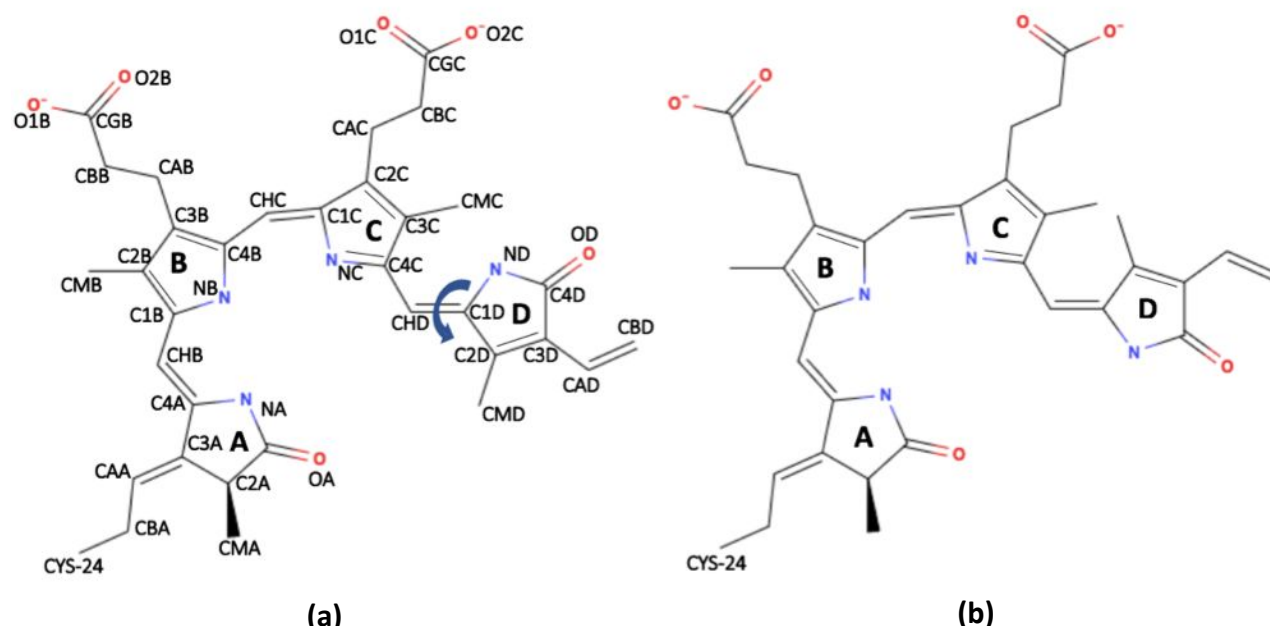


Figure 1. Schematic representation of BV IX α chromophore in the dark (left) and illuminated state (right) phytochrome found in *Deinococcus radiodurans* (DrBphP). The atom naming scheme in (a) is used throughout the text. The figures were generated using MolView v2.2.

In DrBphP, the chromophore is located in the PAS-GAF domain cavity and bound to the protein via a thioether linkage with Cys24 and a hydrogen-bonding network involving residues Asp207,

Arg254, His260, Ser272, Ser274, His290 (The residue numbering is similar to the PDB structures 4O01 and 4O0P).⁸ In the red light absorbing Pr state of DrBphP, the chromophore adopts a ZZZssa geometry, while in the far-red light absorbing Pfr state, it adopts a ZZEssa geometry with an E, anti-conformation for the isomerized D-ring (Figure 1b). Because of these differences in the chromophore conformation, it is widely assumed that photon absorption triggers a photo-isomerization of the D-ring along the CHD=C1D methyl bridge^{4,13,14}. In contrast, non-adiabatic QM dynamics simulations¹⁵ and calculations with different quantum chemical methods suggest that without protein environment the BV isomerization can occur around the CHC=C1C methyl bridge between the B and C rings^{16,17}.

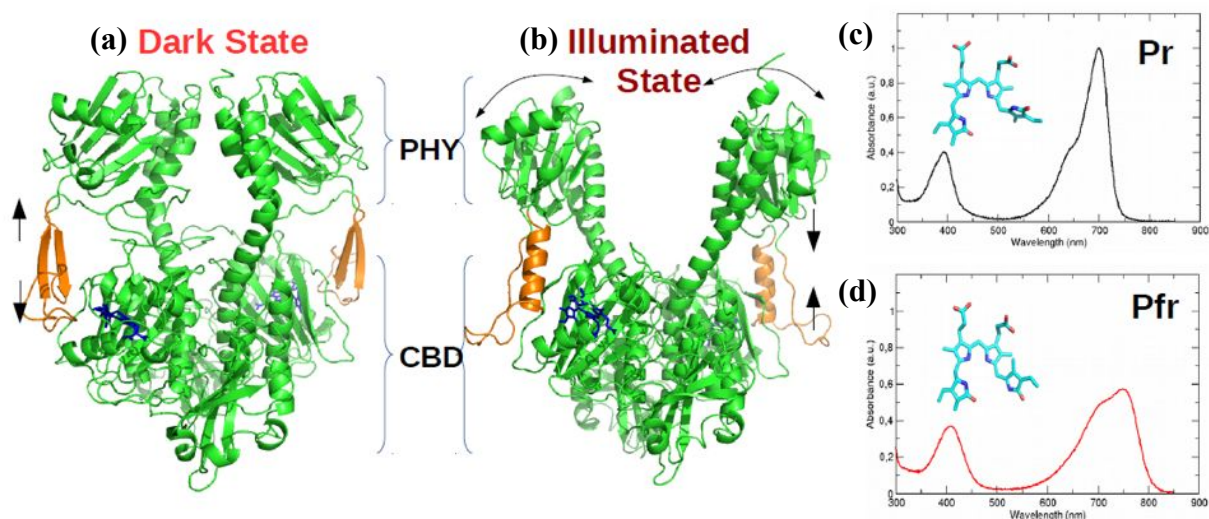


Figure 2. Cartoon representation for the crystal structure of PAS-GAF-PHY domains of DrBphP in (a) Pr-dark state (PDB: 4O0P⁵), that absorbs red-light (700 nm) to trigger the secondary structure rearrangement from β -sheets to α -helix (orange) and a PHY domain opening to form the (b) Pfr-illuminated state (PDB: 4O01⁵) that absorbs a far-red light (750 nm) to revert back to Pr state; (c) and (d) show the experimental UV/Vis absorption spectrum reported by Takala et al., which exhibits the Q-band and Soret-band for Pr and Pfr state, respectively.⁵

Biliverdin photo-isomerization is followed by a series of structural changes in the chromophore binding pocket that ultimately lead to larger structural changes in the protein complex. These major changes include: (i) a secondary structure transformation from an anti-parallel β -sheet to an α -helix in the tongue region (residue range 461-490) between the GAF and PHY domains; and (ii) a large opening of more than ~ 3 nm between the two PHY domains of the dimer in the Pfr state (Figure 2b).⁵ The light-induced changes in the PHY domains are speculated to reposition the HK domain as well as the phosphate-accepting histidine residues in the ATP-binding site within that HK domain.¹⁸ These structural rearrangements would eventually promote a phospho-transfer process within the phytochrome dimer and thereby regulate the downstream signal transmission.¹⁹

The Pr and Pfr x-ray structures (Figure 2a & 2b) provide glimpses of structural changes that follow photo-excitation, but do not address the crucial question of how the protein achieves high signaling efficiency. In addition, there is as yet no consensus about the precise sequence of events in what is essentially a dynamic process. To better understand the molecular mechanisms that drive this reversible photo-activation pathway, experimental data should be complemented with excited-state molecular dynamics simulations, as in previous work on photoreceptors.²⁰⁻²² However, performing such simulations requires an accurate structural model with detailed information about the electrostatic interactions in the chromophore binding pocket, and hence the protonation form of BV.

Various authors have proposed a fully protonated BV in Pr and Pfr state based on H-bond analysis from X-ray crystallography data^{8,9}, NMR experiments^{23,24} and RR spectra^{25,26}. In contrast, others have shown that the Pr \rightarrow Pfr photo-activation includes proton release/uptake^{9,27-33} by the chromophore in the intermediate states with a higher amplitude for the proton release than

uptake^{27,31-33}. While Resonance Raman studies that are sensitive to N-H in-plane vibrations in BV have suggested that the C pyrrole ring nitrogen remains protonated in both Pr and Pfr states of plant and cyanobacterial phytochromes^{25,34,35}, ambiguity remains as to which of the other rings could be involved in these protonation changes. Nevertheless, these observations suggest that in addition to the photo-isomerization also protonation changes may be relevant for photoactivation. Furthermore, because phytochromes from different species vary in (i) their chromophore linkage sites, (ii) orientation of pyrrole rings A/D in both Pr and Pfr state and (iii) isomerization direction of the CHD=C1D double bond³⁶, it remains challenging to reconcile the aforementioned experimental findings into a consistent picture that is valid for phytochromes in general, and DrBphP in particular.

To resolve the chromophore protonation state for DrBphP and prepare an accurate atomistic model for computationally costly excited state molecular dynamics simulations³⁷, we have used classical molecular dynamics (MD) simulations in combination with quantum chemistry and hybrid quantum mechanics / molecular mechanics (QM/MM) calculations to systematically investigate the effect of the chromophore protonation state on the structural and spectroscopic characteristics of DrBphP photo-sensory domain in both Pr and Pfr conformations. Only the five most probable protonation patterns were investigated:

- (1) all nitrogen atoms protonated (all-prot);
- (2) nitrogen in ring A deprotonated, rings B, C and D protonated (deprot-A);
- (3) nitrogen in ring B deprotonated, rings A, C and D protonated (deprot-B);
- (4) nitrogen in ring C deprotonated, rings A, B and D protonated (deprot-C);

(5) nitrogen in ring D deprotonated, rings A, B, and C protonated (deprot-D).

To the best of our knowledge, this is the first study to incorporate the PHY domain along with CBD in MD simulations and QM/MM calculations of DrBphP, aimed at systematically exploring the effects of the chromophore protonation state on the stability and absorptivity of this protein in solution.

In addition, we also assessed the accuracy with which various DFT functionals predict the absorption maxima by comparing the DFT spectra to spectra computed at the correlated multi-configurational level of *ab initio* theory. In line with the assumptions in previous computational studies³⁷⁻⁴⁴, our results support a fully protonated biliverdin chromophore in both Pr and Pfr states of DrBphP, but also suggest that a very minor population, in which the D-ring is deprotonated, might be responsible for a long red-tail in the absorption spectrum of this protein.

Methods

Protein structures

The atomic coordinates of the core photo-sensory module (PAS-GAF-PHY: 523 amino acids) in dark and illuminated state of photo-receptor protein reported by Takala et al., were taken from PDB models 4O0P and 4O0I, with resolutions of 3.80 Å and 3.24 Å, respectively.⁵ Residues missing from these refined X-ray structures (see Table S1 in Supporting Information for an overview of missing residues), were added based on the *ab initio* loop-modelling approach in the MODELLER program^{45,46} that finds the optimal structural model based on a potential energy function. We used the Dowser program to place internal water molecules inside hydrophobic cavities of the protein using a protein-water and water-water interaction energy algorithm.⁴⁷ With

1
2
3 a probe radius of 0.2 Å and new DOWSER parameters for the BV chromophore molecule (Table
4 S2), water molecules were inserted inside protein cavities, in which the interaction energy of the
5
6 water was below a threshold value of -12 kcal/mol (Figure S1).
7
8
9

10
11 The protonation states and tautomeric forms of amino acids with ionizable side chains were
12 determined by pK_a estimation with H++ Server⁴⁸ and PROPKA 3.1^{49,50} at pH=7. The rotameric
13 states of these residues were inspected and modified to a new rotamer if that would increase the
14 number of hydrogen bonds. For amino acids with non-ionizable side chains, the H-atoms were
15 added using force field parameters corresponding to their protonation form at pH=7. As in
16 previous works³⁸⁻⁴¹, we assume the same protonation state of the protein residues for all
17 protonation states of the chromophore. While a change in protonation of the chromophore might
18 affect the pK_a 's of the surrounding protein residues, the number of possible states that would
19 need to be sampled is too large to handle with standard MD simulations and was therefore not
20 attempted here. The structural protein models of the Pr and Pfr states after equilibration are
21 available as supporting information (Pr.pdb and Pfr.pdb).
22
23
24
25
26
27
28
29
30
31
32
33
34
35

36 37 *Force field model* 38 39

40 The AMBER03 force field was used to model interactions between the atoms in our
41 simulations.⁵¹ To model the intra- and intermolecular interactions of the chromophore, we
42 derived force field parameters by means of *ab initio* calculations for a QM model that consisted
43 of BV and the covalently attached side chain of Cys24. For all protonation states the geometry of
44 the QM model was optimized in the gas phase at the CAMB3LYP/6-31G (d, p) level of DFT
45 theory. The partial charges for the different protonation forms of BV were estimated by
46 performing a two-stage Restricted Electrostatic Potential (RESP) fit to the electron density
47
48
49
50
51
52
53
54
55
56
57
58
59
60

obtained at the HF/6-31G(d) level of theory, using constraints on symmetry related atoms in the second step (Table S4-S5).⁵² The atomic charges on the main chain of Cys24 were described following the approach proposed by A. Altun and co-workers (Table S6-S7).⁵³ Additional atom types were created specifically for the chromophore to define new dihedrals and improve structural description. The complete force field for use with the Gromacs molecular dynamics program⁵⁴⁻⁵⁶ is available as supporting information. The DFT and *ab initio* calculations for the RESP fit were carried out with Gaussian09 program⁵⁷ while the actual RESP fittings were performed with the AmberTools15 package⁵⁸.

Classical molecular dynamics simulations

For the MD simulations, the protein was solvated in a cubic periodic box (Pr: 12×12×12 nm and Pfr: 13×13×13 nm), which was filled with TIP3P water molecules.⁵⁹ The large ~3 nm opening of the PHY domain in Pfr state necessitated the larger box size for this system. The total charge on the protein systems was neutralized by replacing solvent water molecules with Na⁺ and Cl⁻ ions until a physiological salt concentration of 0.15 M was reached. The neutral solvated model contained the 81 water molecules added by DOWSER (Figure S1) and another 50,454 and 68,294 water molecules in the Pr and Pfr models, respectively.

The short-range attractive and repulsive dispersive interactions were described by a Lennard-Jones potential with a cut-off of 1.0 nm. Electrostatic interactions were calculated at each time-step using the particle-mesh Ewald (PME) method⁶⁰ with a grid spacing of 0.12 nm. The LINCS algorithm was used to constrain bond lengths in the protein⁶¹, while SETTLE⁶² was used to constrain the internal degrees of freedom of the TIP3P water molecules. These constraints allowed us to perform simulations with a time step of 2 fs.

The ten phytochrome systems were initially subjected to an energy minimization for 10,000 steps using the steepest descent algorithm, followed by multiple equilibration steps: 200 ps simulation with position restrains on all protein atoms and two 500 ps simulations on the position-restrained system using NVT and NPT ensembles for temperature (300K) and pressure (1bar) equilibration, respectively. After minimization and equilibration all phytochrome systems were simulated for 100 ns. All classical MD simulations were performed with GROMACS 4.6.5 MD package⁵⁴⁻⁵⁶.

Spectra calculations

For each chromophore protonation state, a snapshot was taken at every ns from the 100ns trajectories. Single point vertical excitation energies were calculated for these 100 structures at the QM/MM level and superposed into a spectrum. For these QMMM calculations, a smaller BV chromophore QM subsystem (QM-small, Figure S3) was selected, in which the methyl groups of rings-A, B and D and the propionate side chains were replaced by H atoms, and the Cys24 attachment was excluded by truncating the chromophore system at the C3¹-C3² bond. The rest of the system was described at the AMBER03 force field level.⁵¹ In these calculations, electrostatic interactions with the rest of the chromophore, protein and solvent were added to account for the polarization of the QM region by the environment. The choice for a QM subsystem that is smaller than the actual chromophore was validated by comparing the spectra computed for this small QM subsystem to those computed with the complete chromophore plus pyrrole water molecule inside the QM subsystem (Supporting Information, Figures S6).

The excitation energies (ΔE_i) of the snapshots i were computed both at the level of time-dependent density functional theory (TD-DFT)⁶³⁻⁶⁹ and at the correlated multi-configurational level of *ab initio* theory with the extended multi-configuration quasi-degenerate perturbation

theory (XMCQDPT2) method⁷⁰. For the TD-DFT method, we used various functionals (BLYP^{71,72}, B3LYP⁷³⁻⁷⁵, PBE0⁷⁶, and CAMB3LYP⁷⁷) and the 6-31G (d, p) basis set. In the XMCQDPT2 computations, a Complete Active Space Self-Consistent Field (CASSCF) wave function⁷⁸ based on an active space of 12 electrons in 12 orbitals, averaged over first 5 singlet states and expanded in the cc-pVDZ basis set⁷⁹, was used as a reference for the second-order perturbation theory calculation (*i.e.*, XMCQDPT2/SA(5)-CASSCF(12,12)/cc-pVDZ). The active space orbitals used in these calculations are shown in Figure S10 of Supporting Information. The selection of this active space was a trade-off between accuracy and computational efficiency and validated by computing energy profiles for the most relevant chromophore distortions (Figure S11).

The excitation energies were converted into a spectrum by convoluting the energy gaps with Gaussians:

$$I(E) = \sum_i^M \frac{2m_e}{3\hbar^2} \Delta E_i e^{-(E - \Delta E_i)^2 / 2\sigma^2} \mu_i^2$$

where I is the intensity as a function of excitation energy (E), m_e the electron mass, M number of snapshots included in the analysis, ΔE_i the excitation energy in snapshot i and μ_i the transition dipole moment of that excitation. A width of $\sigma = 0.02$ eV was chosen for the convolution. The QM calculations were performed with Gaussian09 package⁵⁷ (DFT and HF) and Firefly⁸⁰ (XMCQDPT2).

We note that a similar approach has recently been used by Polyakov et al.⁴² However, the major difference between their work and ours is that we have computed absorption spectra of ensembles of the protein in solution at room temperature, which can account for possible

heterogeneities that may affect the interpretation of the spectra. In addition, while they focused on the fully protonated chromophore, we also investigated alternative protonation states.

Results and Discussion

Molecular Dynamics simulations

The stability of the chromophore pocket with the different protonation forms of BV was assessed by analyzing the network of non-covalent interactions between the chromophore and the rest of the system in the MD trajectories and comparing these interactions to those in the X-ray structures (Figure 3).

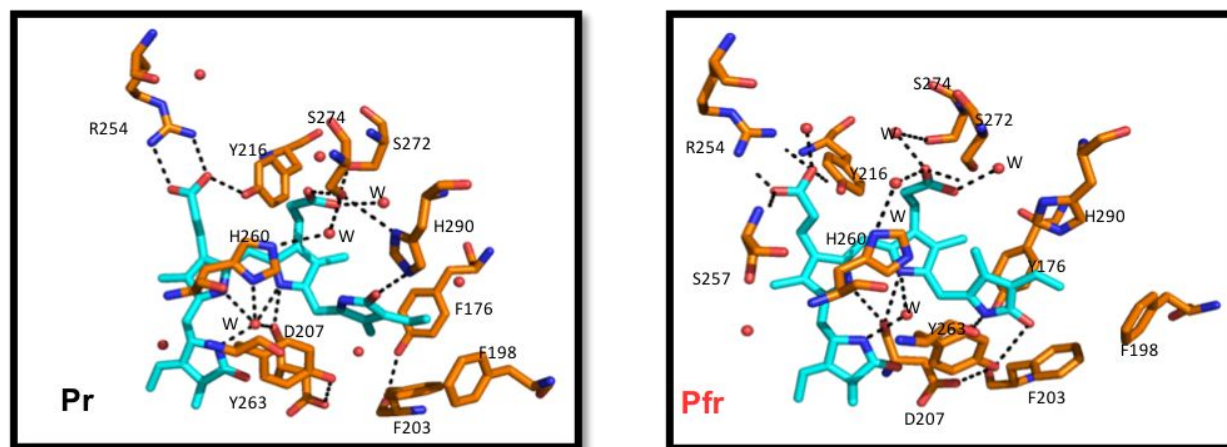


Figure 3. A stick representation of the conserved residues and the H-bonding network surrounding BV. Carbon atoms are colored in cyan and orange for BV and protein, respectively, with nitrogen in blue, oxygen in red and water molecules as red spheres. The hydrogen bonding network for both models of DrBphP is shown as black dashed lines.

Pr - Dark state simulations

The His260 residue stacked below the plane of BV B-ring and C-ring is a stable H-bond acceptor for the pyrrole ring N-H atoms in the all-prot and deprot-D models. In contrast, in the deprot-A,

deprot-B and deprot-C models this interaction breaks off within 25ns and does not reform again (Figure S4). Furthermore, the absence of a proton on the A, B or C ring of chromophore disrupts the electrostatic interaction network involving the BV pyrrole N-atoms, Asp207 backbone carbonyl and the pyrrole water.

The distance distribution of the salt-bridge between the Asp207-Arg466 side-chains (Figure S5) shows least disruptions over 100ns in the all-prot and deprot-D models. In the deprot-A, deprot-B, and deprot-C Pr models, this salt bridge ruptures within the initial 20ns and does not reform in the remainder of the 100ns simulation time.

Hydrophobic residues Phe203, Tyr176 and Tyr263 form a pocket around the D-ring of BV, which allows the D-ring to isomerize without steric clashes between the residue side chains and methyl group on D-ring^{5,8,29}. Altering the interactions involving Tyr176 and Tyr263 causes photo-bleaching in proteins where these amino acids are mutated³⁰. In our Pr simulations with A-ring, B-ring or C-ring deprotonated, the rapid loss of the aforementioned salt bridge between Asp207-Arg466 also disrupts the hydrogen bond between Asp207 and Tyr263 (Figure S5). This rupture causes Tyr263 to move away from Tyr176 and Phe203 and thus destabilizes the whole hydrophobic cavity. In contrast, the cavity remains intact in simulations where the chromophore is fully protonated (all-prot) and deprotonated at the D-ring (deprot-D).

The chromophore B-ring propionate side-chain is stabilized through a salt-bridge with Arg254 and accepts a hydrogen bond from the Tyr216 hydroxyl group. The C-ring propionate side-chain makes polar contacts with S274 and a water mediated contact with His260.^{4,5,8} These propionate side-chain interactions remain intact for all Pr models which suggests a negligible impact of the chromophore protonation on the side-chain interactions (Figure S5).

Pfr - Illuminated state simulations

1
2
3 In the illuminated state, the residue configuration inside the chromophore binding pocket
4 changes due to (i) photo-isomerization, (ii) secondary structure changes in the conserved tongue
5 region in contact with the chromophore and (iii) a global opening of the PHY domain⁵.
6
7
8
9

10
11 The His260, D207, pyrrole water and pyrrole N-atoms of BV form a polar contact network
12 similar to the Pr state in all simulations. The H260 maintains a stable contact with BV pyrrole
13 ring N-atoms by either acting as a hydrogen bond acceptor (all-prot and deprot-D) or donor
14 (deprot-A, deprot-B and deprot-C). However, the conserved interactions Asp207-BV pyrrole N-
15 atoms, Asp207-Ser468 and Ser468-Tyr263 are lost (Figure S6 and S7) in the Pfr state with BV
16 deprotonated at the A, B or C ring. Instead of re-establishing these hydrogen bonds later in the
17 simulation, Asp207 moves out of the chromophore-binding pocket to form new interactions with
18 the solvent molecules. In contrast, when the chromophore is fully protonated or deprotonated at
19 the D-ring, the hydrogen bonds involving Asp207, Ser468 and Tyr263 remain intact. These
20 observations support both a fully protonated chromophore and a chromophore with a
21 deprotonated D ring, rather than the other chromophore protonation states, in which the
22 hydrogen bonds are less stable.
23
24
25
26
27
28
29
30
31
32
33
34
35
36
37
38

39
40 Similar to the Pr state simulations, the B-ring and C-ring propionate side-chain interactions with
41 residues Arg254, Tyr216 and Ser274 are stable in Pfr models regardless of the BV protonation
42 state (Figure S7).
43
44
45
46

47
48 Based on the analysis of the conserved interactions between the chromophore and the protein in
49 our MD simulations, we inferred that the A-ring, B-ring and C-ring are protonated in Pr and Pfr
50 but could not determine whether also the D-ring is protonated, as the chromophore binding
51 pocket was stable in both situations (all-prot and D-deprot model). To differentiate further
52
53
54
55
56
57
58
59
60

1
2
3 between these states, we also computed absorption spectra that can be directly compared to
4
5 experiment.
6

7 8 *Spectra calculations*

9 10 11 *Effect of DFT functional*

12
13
14
15 In figure 4, we compare the UV/vis spectra for Pr with an all-protonated chromophore,
16
17 calculated at various levels of theory. Whereas the TD-DFT spectra contain the Soret band
18
19 around 400 nm and the Q-band around 700 nm, the XMCQDPT2 spectrum lacks a clear Soret
20
21 band. The latter is due to the limited number of states (nstates=5) in the CASSCF calculations.
22
23 With ten states, the Soret band is predicted (Figure S8, Supporting Information), but this is
24
25 computationally too expensive and also not needed as the Q-band absorption near 700 nm is
26
27 much more sensitive to the structural changes associated with photoactivation from Pr to Pfr^{4,5,9}.
28
29
30
31
32
33
34
35
36
37
38
39
40
41
42
43
44
45
46
47
48
49
50
51
52
53
54
55
56
57
58
59
60

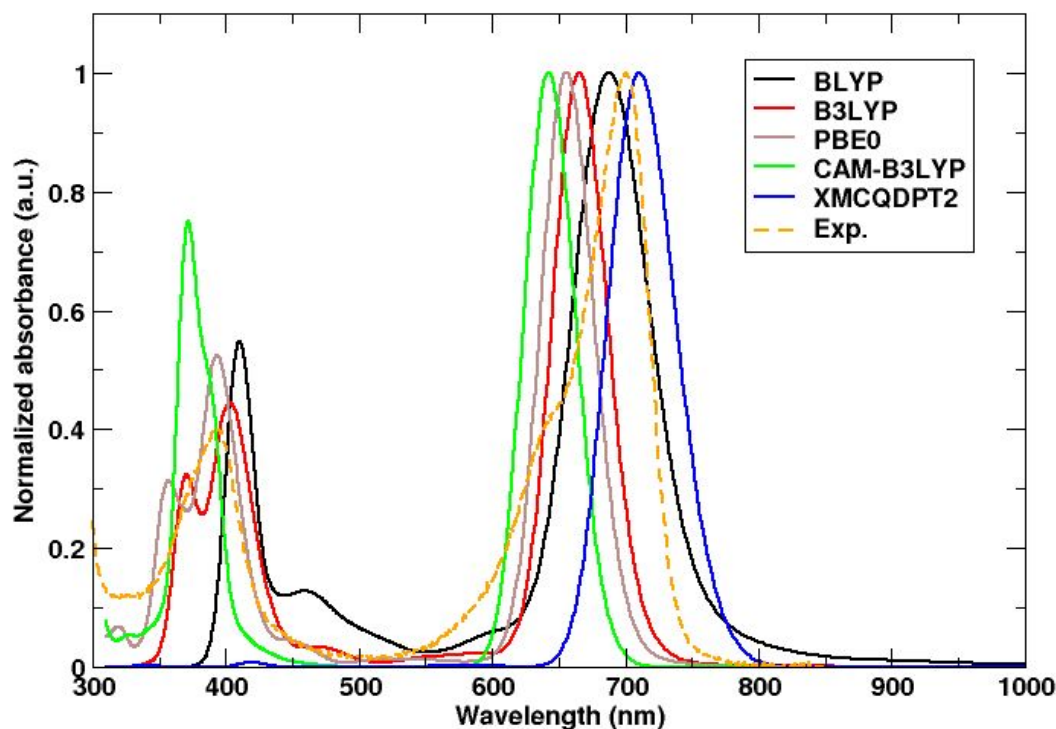


Figure 4. QM/MM UV/vis-absorption spectra of DrBphP evaluated at the TDDFT level with various DFT functionals and at the XMCQDPT2 level of theory in the Pr state. The experimental spectrum is shown in dashed orange lines in both plots, with Q-band peaks at 700 nm and 750 nm for Pr and Pfr state respectively. The best agreement is obtained with the BLYP functional and XMCQDPT2 method with absorption maxima at 692 nm (black line) and 708 nm (blue line), respectively.

Compared to the experimental spectrum with a maximum of the Q-band at 700 nm in the Pr state⁵, the TDDFT spectra are blue-shifted, while the XMCQDPT2 spectrum is red-shifted. The hybrid functionals with 20-25% exact exchange, B3LYP and PBE0, deviated by 35 nm (0.09 eV) and 43 nm (0.116 eV), respectively, while the long-range corrected meta-hybrid CAMB3LYP functional, which was developed to yield more accurate results for charge-transfer excitations, shows the largest blue-shift of 56 nm (0.154 eV). While hybrid functionals and meta-hybrid functionals normally improve the accuracy of electronic excitations involving Rydberg or

charge-transfer states, we here observe that the absorption maximum (692 nm / 1.79 eV) obtained with the GGA BLYP functional is closest to both experiment (700 nm / 1.77 eV) and the XMCQDPT2 result (708 nm / 1.75 eV). The performance of the different DFT functionals for the CBD-PHY dimer are in line with the results of a recent benchmark study on the CBD monomer.⁴⁰ Because of the better agreement of the TD-BLYP/6-31G(d) and the XMCQDPT2/cc-pVDZ results for Pr, we only consider these methods in what follows.

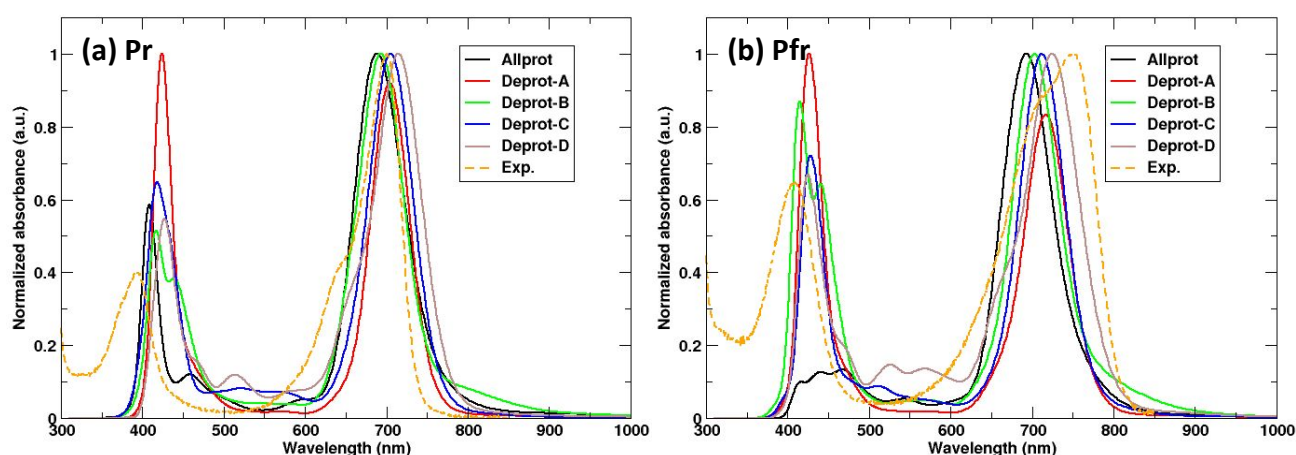


Figure 5: Compute UV/Vis absorption spectra of the photo-active states models Pr and Pfr with different protonation form of BV chromophore computed using TD-DFT method, BLYP/6-31G(d,p).

TDDFT/MM spectra of various protonation states

Based on the analysis of the conserved interactions between the chromophore and the protein in our MD simulations, we inferred that the A-ring, B-ring and C-ring are protonated, but could not determine whether also the D-ring is protonated, as the chromophore binding pocket was stable in both situations (all-prot and D-deprot model). Therefore, we compare the computed absorption spectra of the five chromophore protonation states to experiments. Figure 5 shows these absorption spectra for both Pr and Pfr protein conformations. While in experiments the photo-

activation of DrBphP is accompanied by a red-shift in the Q-band absorption of 0.12 eV (from 700 to 750 nm), our TD-DFT/MM calculations show much smaller red-shifts. The largest red-shift (0.04 eV) was obtained when the chromophore D-ring is deprotonated, in which case the absorption maximum changes from 714 in Pr to 731 nm in Pfr. With the fully protonated chromophore the red-shift is much smaller: only 8 nm or 0.02 eV. The maximum shift, however, is obtained if we assume that somewhere along the Pr to Pfr transition, the D ring becomes deprotonated. In this scenario, the Q-band absorption maximum moves from 688 nm in the Pr state to 731 nm in the Pfr state, which corresponds to a red-shift of 0.11 eV (43 nm), in reasonable agreement with experiment. Previously, such loss of a proton has been suggested to occur during the Pr-to-Pfr conversion in cyanobacterial phytochromes Cph1 and bacterial phytochromes Agp1 on the basis of flash-induced transient absorption measurements and pH dependence of the absorption spectra^{27-30,33,34}. Based on the MD snapshot in Figure S13, which highlights a proton wire from the chromophore to solvent, we speculate that the proton could leave the pyrrole D-ring of BV via that wire. Alternatively, also His260 might be involved, as it could potentially shuttle the proton onto the pyrrole water molecule, which exchanges frequently with bulk solvent in both Pr and Pfr simulations.

At this point, the combined MD simulations and TDDFT/MM calculations suggest a protonated chromophore in the Pr state of DrBphP and a chromophore that is deprotonated at the D-ring in the Pfr state. However, because the systematic error in TDDFT of about 0.25 eV⁸¹ is beyond the measurable red-shift, further confirmation is essential. We therefore also computed the absorption spectra at the correlated XMCQDPT2 level of theory, which has a higher accuracy with an error of about 0.1 eV⁷⁰.

Table 1. Q-band and Soret-band peak computed from single point excited state energies using BLYP/6-31G (d,p) for 5 different protonation forms of BV in both Pr and Pfr states.

BV protonation form	Pr – Dark state (nm)		Pfr- Illuminated state (nm)	
	Q-band	Soret-band	Q-band	Soret-band
All-prot	696	409	704	476
Deprot-A	708	421	720	433
Deprot-B	696	439	708	413
Deprot-C	712	416	716	424
Deprot-D	716	430	742	423
Exp.	700	394	750	409

XMCQDPT2 spectra

In previous works the effect of deprotonation at the A, B and C rings on the optical response of the chromophore has been computed^{14,37,41,43}, but not at the D-ring. Since we rule out deprotonation of the A, B and C rings in both the Pr and Pfr states of the photo-sensory domain based on the MD simulations, we have not computed the excitation spectra for these species at XMCQDPT2 level of theory. The XMCQDPT2/SA (5)-CASSCF(12,12)/cc-pVDZ//Amber03 QM/MM spectra are shown in Figure 6. While for the fully protonated chromophore the spectra agree reasonably with the TD-BLYP results (Figure 5 and 6), the spectrum of the protein with a chromophore that is deprotonated at the D-ring, shows additional peaks. In particular, there is a broad optical transition beyond 800 nm that was not seen in the TD-DFT computations. Inspection of the molecular orbitals involved in these excitations reveals that the lowest-energy S_0 - S_1 transition in the deprotonated chromophore at 850 nm corresponds to a single electron HOMO-LUMO transition, while the excitation around 700 nm is a two-electron, or double excitation. Due to the adiabatic approximation in the exchange-correlation response kernel

(ALDA), these double excitations are notoriously difficult to describe with TD-DFT, which is why they are missing here. The apparent agreement between the TD-DFT results and experiment must thus have been fortuitous and therefore cannot be used to support that the D-ring of the chromophore is deprotonated in either Pfr or Pr. Consistent with the TD-DFT results, the redshift between the Pr and Pfr states with the fully protonated chromophore is underestimated also at the XMCQDPT2/cc-pVDZ level (0.032 eV), but the deviation with respect to the experimental absorption maximum (0.12 eV) is closer to the anticipated error of the method (~ 0.1 eV)⁷⁰.

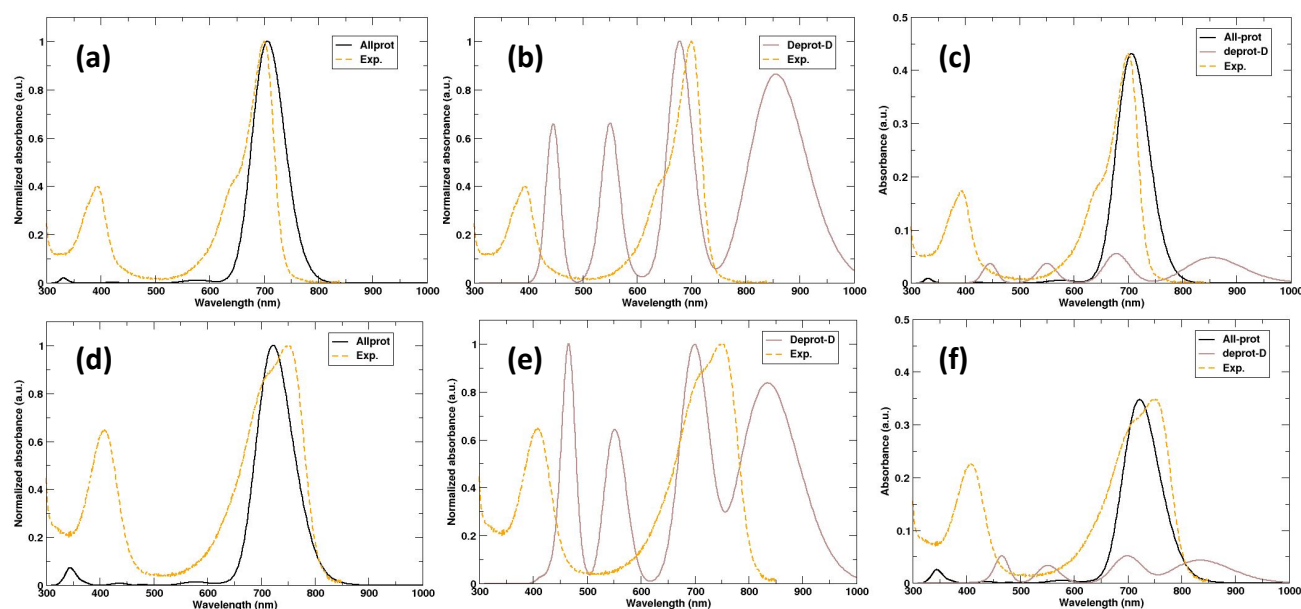


Figure 6. Calculated UV/Vis absorption spectra for the fully protonated BV model ((a)-Pr, (d)-Pfr) and model with the D-ring deprotonated ((b)-Pr, (e)-Pfr) of DrBphP at the correlated XMCQDPT2 level of theory. Plots (c) and (f) represent the unnormalized spectra for the Pr and Pfr states, respectively, where the experimental spectra were scaled to the peak of the fully protonated BV model for better comparison.

However, before concluding that the chromophore is fully protonated in both Pr and Pfr states of the protein, we notice that due to the much lower oscillator strength of the chromophore with

deprotonated D-ring (Figure 6), the spectrum would be dominated by absorption of the protonated chromophore, masking the deprotonated species. Furthermore, the spectra available in the literature for this protein were only recorded up until 850 nm and sometimes even baseline corrected⁴⁻⁷. Therefore, we speculate that in particular the red-tail of the absorption might contain a minor contribution from proteins, in which the D-ring is not protonated. An indication in support of our speculation are the spectra of phytochromes with covalently modified biliverdin chromophores, which show a weak, but visible rise in absorption beyond 850 nm^{82,83}. Nevertheless, to experimentally verify whether the deprotonated chromophore indeed absorbs beyond 850 nm, we suggest recording the spectra over a larger range of wave lengths and pH values.

Conclusion

We have performed MD simulations of the photo-sensory domain of the *Deinococcus radiodurans* phytochrome protein with five different biliverdin protonation states in an attempt to determine the most likely protonation state. An analysis of the trajectories in terms of chromophore-protein interactions as well as absorption spectra suggest that the biliverdin chromophore in DrBphP is fully protonated, in line with previous assumptions. However, based on the QM/MM spectra calculations at the correlated level of theory, we cannot rule out a minor population of proteins containing a chromophore with deprotonated the D-ring. Therefore, in our follow-up work, aimed at unravelling the photo-isomerization mechanism, we will not only perform excited state dynamics simulations of the protein with a fully protonated chromophore, but also include simulations in which the D-ring of the chromophore is deprotonated. Because we found that the optical S_0 - S_1 transition of the latter has double excitation character, we will need a suitable multi-configurational method rather than a TD-DFT model.

AUTHOR INFORMATION

Corresponding Author

*dmitry.morozov@jyu.fi

Author Contributions

The manuscript was written through contributions of all authors. All authors have given approval to the final version of the manuscript.

Funding Sources

This work was funded by the Academy of Finland (Grant 304455 to GG and VM, Grant 285481 to DM, and Grant 266274 to SD).

ACKNOWLEDGMENTS

We want to thank Janne Ihalainen, Heli Lehtivuori, Jessica Rumsfeld, Heikki Takala and Sebastian Westenhof for fruitful discussions. We thank Heikki Takala for sharing the absorption spectra and Alex Bjorling for sharing the details of their phytochrome simulations. We also acknowledge the Finnish Grid and Cloud Infrastructure (persistent identifier urn:nbn:fi:research-infras-2016072533), the CSC-IT center in Espoo, Finland and PRACE (DECI-13) for awarding us access to resource at Cartesius in Dutch facility SURFsara for providing computational resources for the MD simulations. Molecular structure figures were generated using MolView v2.4 and PyMOL⁸⁵.

ABBREVIATIONS

TD-DFT, time-dependent density function theory; XMCQDPT2, extended multiconfigurational quasi-degenerate perturbation theory; DrBphP, *Deinococcus radiodurans* phytochrome; BV, Biliverdin; MD, molecular dynamics; QM/MM, quantum mechanics/molecular mechanics.

SUPPORTING INFORMATION

Additional data and figures including the molecular modelling parameters, force field parameterization of BV chromophore, distance distribution analysis of MD simulations based on non-covalent interactions, Soret-band peaks computed using XMCQDPT2 method, comparison for different sizes of the QM subsystem, CASSCF(12,12) active space orbitals generated for the XMCQDPT2 excited state energy calculations, excited-state relaxed energy scans of the most important biliverdin torsions, proton release/uptake pathway, and the effect of the including Range-Separation on the chromophore force field (PDF). Equilibrated structure models of Pr and Pfr states for MD simulations as separate files (PDB). GROMACS 4.6.5 compatible AMBER03 force field parameters files for 10 different BV chromophore models as separate archive (ZIP).

REFERENCES

1. Sineshchekov, V.A. Photobiophysics and Photobiochemistry of the Heterogeneous Phytochrome system. *Biochimica et Biophysica Acta (BBA)-Bioenergetics*. **1995**, 1228, 125-164.
2. Davis, S. J.; Vener, A. V.; Vierstra, R. D. Bacteriophytochromes: Phytochrome-Like Photoreceptors from Nonphotosynthetic Eubacteria. *Science*. **1999**, 286, 2517–2520.

3. Quail, P. H. Phytochrome Photosensory Signalling Networks. *Nature reviews Molecular Cell Biology*. **2002**, 3, 85–93.
4. Rockwell, Nathan C.; Yi-Shin Su; J. Clark Lagarias. Phytochrome Structure and Signaling Mechanisms. *Annual Review Plant Biology*. **2006**, 57, 837–858.
5. Takala, H.; Björling, A.; Berntsson, O.; Lehtivuori, H.; Niebling, S.; Hoernke, M.; Kosheleva, I.; Henning, R.; Menzel, A.; Ihalainen, J. A. et al. Signal Amplification and Transduction in Phytochrome Photosensors. *Nature*. **2014**, 509, 245–8.
6. Giraud, E.; Fardoux, J.; Fourier, N.; Hannibal, L.; Gently, B.; Bouyer, P.; Dreyfus, B.; Verméglio, A. Bacteriophytochrome Controls Photosystem Synthesis in Anoxygenic Bacteria. *Nature*. **2002**, 417, 202-205.
7. Tasler, R.; Moises, T.; Frankenberg-Dinkel, N. Biochemical and Spectroscopic Characterization of the Bacterial Phytochrome of *Pseudomonas aeruginosa*. *The FEBS Journal*. **2005**, 272, 1927-36.
8. Wagner, J. R.; Brunzelle, J. S.; Forest, K. T.; Vierstra, R. D. A Light-Sensing Knot Revealed by the Structure of the Chromophore-Binding Domain of Phytochrome. *Nature*. **2005**, 438, 325–331.
9. Burgie, E. S.; Zhang, J.; Vierstra, R. D. Crystal Structure of Deinococcus Phytochrome in the Photoactivated State Reveals a Cascade of Structural Rearrangements During Photoconversion. *Structure*. **2016**, 24, 448–457.
10. Rockwell, N. C.; Njuguna, S. L.; Roberts, L.; Castillo, E.; Parson, V. L.; Dwojak, S.; Lagarias, J. C.; Spiller, S. C. A Second Conserved GAF Domain Cysteine is Required for

- the Blue/Green Photoreversibility of Cyanobacteria Tlr0924 from *Thermosynechoccus elongatus*. *Biochemistry*. **2008**, *47*, 7304–7316.
11. Essen, L.O.; Mailliet, J.; Hughes, J. The Structure of a Complete Phytochrome Sensory Module in the Pr Ground State. *Proceedings of the National Academy of Sciences*. **2008**, *105*, 14709-14.
12. Lamparter, T. Evolution of Cyanobacterial and Plant Phytochromes. *FEBS Letters*. **2004**, *573*, 1-5.
13. Vierstra, R. D.; Karniol, B. In Handbook of Photosensory Receptors; Briggs, W., Spudich, J., Eds.; Wiley-VCH Press: Weinheim, Germany, **2005**; 171–196.
14. Falklöf, O.; Durbeej, B. Steric Effects Govern the Photoactivation of Phytochromes. *ChemPhysChem*. **2016**, *17*, 954-7.
15. Zhuang, X.; Wang, J.; Lan, Z. Tracking of the Molecular Motion in the Primary Event of Photoinduced Reactions of a Phytochromobilin Model. *The Journal of Physical Chemistry B*. **2013**, *117*, 15976-86.
16. Durbeej, B. On the Primary Event of Phytochrome: Quantum Chemical Comparison of Photoreactions at C4, C10 and C15. *Physical Chemistry Chemical Physics*. **2009**, *11*, 1354-61.
17. Strambi, A.; Durbeej, B. Initial Excited-State Relaxation of the Bilin Chromophores of Phytochromes: A Computational Study. *Photochemical & Photobiological Sciences*. **2011**, *10*, 569-579.

18. Björling, A.; Berntsson, O.; Lehtivuori, H.; Takala, H.; Hughes, A.J.; Panman, M.; Hoernke, M.; Biebling, A.; Henry, L.; Henning, R. et al. Structural Photoactivation of a Full-Length Bacterial Phytochrome. *Science Advances*. **2016**, *2*, p.e1600920.
19. Li, H.; Zhang, J.; Vierstra, R. D.; Li, H. Quaternary Organization of a Phytochrome Dimer as Revealed by Cryoelectron Microscopy. *Proceeding of the National Academy of Sciences*. **2010**, *107*, 10872–10877.
20. Pande, K.; Hutchison, C. D. M.; Groenhof, G.; Aquila, A.; Robinson, J. S.; Tenboer, J.; Basu, S.; Boutet, S.; DePonte, D. P.; Liang, M. et al. Femtosecond Structural Dynamics Drives the trans/cis Isomerization in Photoactive Yellow Protein. *Science*. **2016**, *352*, 725–729.
21. Polli, D.; Altoè, P.; Weingart, O.; Spillane, K. M.; Manzoni, C.; Brida, D.; Tomasello, G.; Orlandi, G.; Kukura, P.; Mathies, R. A.; Garavelli, M. Conical Intersection Dynamics of the Primary Photoisomerization Event in Vision. *Nature*. **2010**, *467*, 440.
22. Gozem, S.; Luk, H. L.; Schapiro, I.; Olivucci, M. Theory and Simulation of the Ultrafast Double-Bond Isomerization of Biological Chromophores. *Chemical Reviews*. **2017**, *117*, 13502-65.
23. Strauss, H. M.; Hughes, J.; Schmieder, P. Heteronuclear Solution-State NMR Studies of the Chromophore in Cyanobacterial Phytochrome Cph1. *Biochemistry*. **2005**, *44*, 8244–8250.
24. Rohmer, T.; Strauss, H. M.; Hughes, J.; De Groot, H.; Gärtner, W.; Schmieder, P.; Matysik, J. 15N MAS NMR Studies of Cph1 Phytochrome: Chromophore Dynamics and

- Intramolecular Signal Transduction. *The Journal of Physical Chemistry B*. **2006**, *110*, 20580–20585.
25. Kneip, C.; Hildebrandt, P.; Németh, K.; Mark, F.; Schaffner, K. Interpretation of the resonance Raman Spectra of Linear Tetrapyrroles Based on DFT Calculations. *Chemical Physics Letters*. **1999**, *311*, 479–484.
26. Von Stetten, D.; Günther, M.; Scheerer, P.; Murgida, D. H.; Mroginski, M. A.; Krauß, N.; Lamparter, T.; Zhang, J.; Anstrom, D. M.; Vierstra, R. D.; Forest, K. T.; Hildebrandt, P. Chromophore Heterogeneity and Photoconversion in Phytochrome Crystals and Solution Studied by Resonance Raman Spectroscopy. *Angewandte Chemie International Edition*. **2008**, *47*, 4753–4755.
27. Van Thor, J. J.; Borucki, B.; Crielard, W.; Otto, H.; Lamparter, T.; Hughes, J.; Hellingwerf, K. J.; Heyn, M. P. Light-Induced Proton Release and Proton Uptake Reactions in the Cyanobacterial Phytochrome Cph1. *Biochemistry*. **2001**, *40*, 11460–11471.
28. Borucki, B.; Von Stetten, D.; Seibeck, S.; Lamparter, T.; Michael, N.; Mroginski, M. A.; Otto, H.; Murgida, D. H.; Heyn, M. P.; Hildebrandt, P. Light-Induced Proton Release of Phytochrome is Coupled to the Transient Deprotonation of the Tetrapyrrole Chromophore. *Journal of Biological Chemistry*. **2005**, *280*, 34358–34364.
29. Von Stetten, D.; Seibeck, S.; Michael, N.; Scheerer, P.; Mroginski, M. A.; Murgida, D. H.; Krauß, N.; Heyn, M. P.; Hildebrandt, P.; Borucki, B.; Lamparter, T. Highly Conserved Residues Asp-197 and His-250 in Agp1 Phytochrome Control the Proton

- Affinity of the Chromophore and Pfr Formation. *Journal of Biological Chemistry*. **2007**, 282, 2116–2123.
30. Wagner, J. R.; Zhang, J.; Von Stetten, D.; Günther, M.; Murgida, D. H.; Mroginski, M. A.; Walker, J. M.; Forest, K. T.; Hildebrandt, P.; Vierstra, R. D. Mutational Analysis of *Deinococcus radiodurans* Bacteriophytochrome Reveals Key Amino Acids Necessary for the Phtotochromicity and Proton Exchange Cycles of Phytochrome. *Journal of Biological Chemistry*. **2008**, 283, 12212–12226.
31. Borucki, B.; Seibeck, S.; Heyn, M. P.; Lamparter, T. Characterization of the Covalent and Noncovalent Adducts of Agp1 Phytochrome Assembled With Biliverdin and Phycocyanobilin by Circular Dichroism and Flash Photolysis. *Biochemistry*. **2009**, 48, 6305-17.
32. Escobar, F. V.; Piwowarski, P.; Salewski, J.; Michael, N.; Lopez, M. F.; Rupp, A.; Qureshi, B. M.; Scheerer, P.; Bartl, F.; Frankenberg-Dinkel, N.; Siebert, F. A Protonation-Coupled Feedback Mechanism Controls the Signalling Process in Bathy Phytochromes. *Nature Chemistry*. **2015**, 7, 423-30.
33. Escobar F. V.; Lang, C.; Takiden, A.; Schneider, C.; Balke, J.; Hughes, J.; Alexiev, U.; Hildebrandt, P.; Mroginski, M. A. Protonation-Dependent Structural Heterogeneity in the Chromophore Binding Site of Cyanobacterial Phytochrome Cph1. *The Journal of Physical Chemistry B*. **2016**, 121, 47-57.
34. Matysik, J.; Hildebrandt, P.; Schlamann, W.; Braslavsky, S.; Schaffner, K. Fourier-Transform Resonance Raman Spectroscopy of Intermediates of the Phytochrome Photocycle. *Biochemistry*. **1995**, 34, 10497-507.

35. Kneip C, Hildebrandt P, Schlamann W, Braslavsky SE, Mark F, Schaffner K. Protonation State and Structural Changes of the Tetrapyrrole Chromophore During the Pr→ Pfr Phototransformation of Phytochrome: A Resonance Raman Spectroscopic Study. *Biochemistry*. **1999**, 38, 15185-92.
36. Rockwell, N. C.; Shang, L.; Martin, S. S.; Lagarias, J. C. Distinct Classes of Red/Far-red Photochemistry Within the Phytochrome Superfamily. *Proceedings of the National Academy of Sciences*. **2009**, 106, 6123–6127.
37. Boggio-Pasqua, M.; Burmeister, C. F.; Robb, M. A.; Groenhof, G. Photochemical Reactions in Biological Systems: Probing the Effect of the Environment by Means of Hybrid Quantum Chemistry/Molecular Mechanics Simulations. *Physical Chemistry Chemical Physics*. **2012**, 14, 7912-28.
38. Durbeej, B.; Borg, O. A.; Eriksson, L. A. Computational Evidence in Favor of a Protonated Chromophore in the Photoactivation of Phytochrome. *Chemical Physics Letters*. **2005**, 416, 83-88.
39. Matute, R. A.; Contreras, R.; González, L. Time-dependent DFT on Phytochrome Chromophores: A Way to the Right Conformer. *The Journal of Physical Chemistry Letters*. **2010**, 1, 796–801.
40. Falklöf, O.; Durbeej, B. Modeling of Phytochrome Absorption Spectra. *Journal of Computational Chemistry*. **2013**, 34, 1363-1374.

41. Falklöf, O.; Durbeej, B. Computational Identification of Pyrrole Ring C as the Preferred Donor for Excited-State Proton Transfer in Bacteriophytochromes. *ChemPhotoChem*. 2018, **2**, 453-7.
42. Polyakov, I. V.; Grigorenko, B. L.; Mironov, V. A.; Nemukhin, A. V. Modeling Structure and Excitation of Biliverdin-Binding Domains in Infrared Fluorescent Proteins. *Chemical Physics Letters*. **2018**, *710*, 59-63.
43. Feliks, M.; Lafaye, C.; Shu, X.; Royant, A.; Field, M. Structural Determinants of Improved Fluorescence in a Family of Bacteriophytochrome-Based Infrared Fluorescent Proteins: Insights from Continuum Electrostatic Calculations and Molecular Dynamics Simulations. *Biochemistry*. **2016**, *55*, 4263-74.
44. Hasegawa, J. Y.; Isshiki, M.; Fujimoto, K.; Nakatsuji, H. Structure of Phytochromobilin in the Pr and Pfr Forms: SAC-CI Theoretical Study. *Chemical Physics Letters*. **2005**, *410*, 90-93.
45. Šali, A.; Blundell, T. L. Comparative Protein Modelling by Satisfaction of Spatial Restraints. *Journal of Molecular Biology*. **1993**, *234*, 779–815.
46. Fiser, A.; Do, R. K. G.; Šali, A. Modelling of Loops in Protein Structures. *Protein Science*. **2000**, *9*, 1753–1773.
47. Zhang, L.; Hermans, J. Hydrophilicity of Cavities in Proteins. *Proteins Structure, Function and Bioinformatics*. **1996**, *24*, 433–438.

48. Anandakrishnan, R.; Aguilar, B.; Onufriev, A. V. H++ 3.0: Automating pK Prediction and the Preparation of Biomolecular Structures for Atomistic Molecular Modeling and Simulations. *Nucleic Acids Research*. **2012**, *40*, W537–W541.
49. Søndergaard, C. R.; Olsson, M. H. M.; Rostkowski, M.; Jensen, J. H. Improved Treatment of Ligands and Coupling Effects in Empirical Calculation and Rationalization of pKa Values. *Journal of Chemical Theory and Computation*. **2011**, *7*, 2284–2295.
50. Olsson, M. H. M.; Søndergaard, C. R.; Rostkowski, M.; Jensen, J. H. PROPKA3: Consistent Treatment of Internal and Surface Residues in Empirical pKa Predictions. *Journal of Chemical Theory and Computation*. **2011**, *7*, 525–537.
51. Duan, Y.; Wu, C.; Chowdhury, S.; Lee, M.C.; Xiong, G.; Zhang, W.; Yang, R.; Cieplak, P.; Luo, R.; Lee, T. Caldwell, J. A Point-Charge Force Field for Molecular Mechanics Simulations of Proteins Based on Condensed-Phase Quantum Mechanical Calculations. *Journal of Computational Chemistry*. **2003**, *24*, 1999–2012.
52. Bayly, C. I.; Cieplak, P.; Cornell, W. D.; Kollman, P. A. A Well-Behaved Electrostatic Potential Based Method Using Charge Restraints for Deriving Atomic Charges: the RESP Model. *The Journal of Physical Chemistry*. **1993**, *97*, 10269–10280.
53. Altun, A.; Yokoyama, S.; Morokuma, K. Spectral Tuning in Visual Pigments: An ONIOM (QM: MM) Study on Bovine Rhodopsin and its Mutants. *The Journal of Physical Chemistry B*. **2008**, *112*, 6814–6827.

54. Hess, B.; Kutzner, C.; van der Spoel, D.; Lindahl, E. GROMACS 4: Algorithms for Highly Efficient, Load-Balanced, and Scalable Molecular Simulation. *Journal of Chemical Theory and Computation*. **2008**, *4*, 435–447.
55. Pronk, S.; Páll, S.; Schulz, R.; Larsson, P.; Bjelkmar, P.; Apostolov, R.; Shirts, M. R.; Smith, J. C.; Kasson, P. M.; van der Spoel, D.; Hess, B. GROMACS 4.5: A High-Throughput and Highly Parallel Open Source Molecular Simulation Toolkit. *Bioinformatics*. **2013**, *29*, 845-54.
56. Van Der Spoel, D.; Lindahl, E.; Hess, B.; Groenhof, G.; Mark, A. E.; Berendsen, H. J. GROMACS: Fast, Flexible, and Free. *Journal of Computational Chemistry*. **2005**, *26*, 1701-18.
57. Frisch, M. J.; Trucks, G. W.; Schlegel, H. B.; Scuseria, G. E.; Robb, M. A.; Cheeseman, J. R.; Scalmani, G.; Barone, V.; Mennucci, B.; Petersson, G. A. et al. Gaussian 09, Revision D.01; Gaussian, Inc.; Wallingford CT, **2009**.
58. Case, D.A.; Berryman, J.T.; Betz, R.M.; Cerutti, D.S.; Cheatham, T.E.; Darden, III, T.A.; Duke, R.E.; Giese, T.J.; Gohlke, H.; Goetz, A.W. et al. AMBER 2015, University of California, San Francisco, **2015**.
59. Jorgensen, W.L.; Chandrasekhar, J.; Madura, J.D.; Impey, R.W. and Klein, M.L. Comparison of Simple Potential Functions for Simulating Liquid Water. *The Journal of Chemical Physics* **1983**, *79*, 926-935.

60. Essmann, U.; Perera, L.; Berkowitz, M.L.; Darden, T.; Lee, H. and Pedersen, L.G.; A Smooth Particle Mesh Ewald Method. *The Journal of Chemical Physics*. **1995**, *103*, 8577-8593.
61. Hess, B.; Bekker, H.; Berendsen, H. J.; Fraaije, J. G. LINCS: A Linear Constraint Solver for Molecular Simulations. *Journal of Computational Chemistry*. **1997**, *18*, 1463-72.
62. Miyamoto, S.; Kollman, P. A. SETTLE: An Analytical Version of the SHAKE and RATTLE Algorithm for Rigid Water Models. *Journal of Computational Chemistry*. **1992**, *13*, 952-962.
63. Bauernschmitt, R.; Ahlrichs, R. Treatment of Electronic Excitations Within the Adiabatic Approximation of Time Dependent Density Functional Theory. *Chemical Physics Letters*. **1996**, *256*, 454-64.
64. Casida, M. E.; Jamorski, C.; Casida, K. C.; Salahub, D. R. Molecular Excitation Energies to High-Lying Bound States from Time-Dependent Density-Functional Response Theory: Characterization and Correction of the Time-Dependent Local Density Approximation Ionization Threshold. *The Journal of Chemical Physics*. **1998**, *108*, 4439-49.
65. Stratmann, R. E.; Scuseria, G. E.; Frisch, M. J. An Efficient Implementation of Time-Dependent Density-Functional Theory for the Calculation of Excitation Energies of Large Molecules. *The Journal of Chemical Physics*. **1998**, *109*, 8218-24.
66. Furche, F.; Ahlrichs, R. Adiabatic Time-Dependent Density Functional Methods for Excited State Properties. *The Journal of Chemical Physics*. **2002**, *117*, 7433-47.

67. Casida, M. E. Time-Dependent Density-Functional Theory for Molecules and Molecular Solids. *Journal of Molecular Structure: THEOCHEM*. **2009**, *914*, 3-18.
68. Adamo, C.; Jacquemin, D. The Calculations of Excited-State Properties with Time-Dependent Density Functional Theory. *Chemical Society Reviews*. **2013**, *42*, 845-56.
69. Dreuw, A.; Head-Gordon, M. Single-Reference Ab initio Methods for the Calculation of Excited States of Large Molecules. *Chemical Reviews*. **2005**, *105*, 4009-37.
70. Granovsky, A. A. Extended Multi-Configuration Quasi-Degenerate Perturbative Theory: The New Approach to Multi-State Multi-Reference Perturbation Theory. *The Journal of Chemical Physics*. **2011**, *134*, 214113.
71. Becke, A. D. Density-Functional Exchange-Energy Approximation with Correct Asymptotic Behavior. *Physical Review A*. **1988**, *38*, 3098.
72. Lee, C.; Yang, W.; Parr, R. G. Development of Colle-Salvetti Correlation-Energy Formula into a Functional of the Electron Density. *Physical Review B*. **1988**, *37*, 785-789.
73. Becke, A. D. Density-Functional Thermochemistry. III. The Role of Exact eExchange. *The Journal of Chemical Physics*. **1993**, *98*, 5648-5652.
74. Vosko, S. H.; Wilk, L.; Nusair, M. Accurate Spin-Dependent Electron Liquid Correlation Energies for Local Spin Density Calculations: A Critical Analysis. *Canadian Journal of Physics*. **1980**, *58*, 1200-1211.
75. Stephens, P. J.; Devlin, F. J.; Chabalowski, C. F.; Frisch, M. J. Ab initio Calculation of Vibrational Absorption and Circular Dichroism Spectra Using Density Functional Force Fields. *The Journal of Physical Chemistry*. **1994**, *98*, 11623-11627.

76. Adamo, C.; Barone, V. Toward Reliable Density Functional Methods Without Adjustable Parameters: The PBE0 Model. *The Journal of Chemical Physics*. **1999**, *110*, 6158-6170.
77. Yanai, T.; Tew, D. P.; Handy, N. C. A New Hybrid Exchange-Correlation Functional Using the Coulomb-Attenuating Method (CAM-B3LYP). *Chemical Physics Letters*. **2004**, *393*, 51-57.
78. Roos, B. O.; Taylor, P. R.; Si, P. E. A Complete Active Space SCF Method (CASSCF) Using a Density Matrix Formulated Super-CI Approach. *Chemical Physics*. **1980**, *48*, 157-73.
79. Dunning, Jr. T. H. Gaussian Basis Sets for Use in Correlated Molecular Calculations. I. The Atoms Boron Through Neon and Hydrogen. *The Journal of Chemical Physics*. **1989**, *90*, 1007-23.
80. Granovsky, A. A. Firefly version 8.2. Available at: <http://classic.chem.msu.su/gran/firefly/index.html>. Accessed 20 September 2017.
81. Jacquemin, D.; Wathelet, V.; Perpète, E. A.; Adamo, C. Extensive TD-DFT Benchmark: Singlet-Excited States of Organic Molecules. *Journal of Chemical Theory and Computation*. **2009**, *5*, 2420-35.
82. Inomata, K.; Hammam, M. A.; Kinoshita, H.; Murata, Y.; Khawn, H.; Noack, S.; Michael, N.; Lamparter, T. Sterically Locked Synthetic Bilin Derivatives and Phytochrome Agp1 from *Agrobacterium tumefaciens* form Photoinsensitive Pr-and Pfr-Like Adducts. *Journal of Biological Chemistry*. **2005**, *280*, 24491-97.

- 1
2
3 83. Rockwell, N. C.; Lagarias, J. C. The Structure of Phytochrome: A Picture is Worth a
4
5 Thousand Spectra. *The Plant Cell*. **2006**, *18*, 4-14.
6
7
8
9 84. Ihalainen, J. A.; Gustavsson, E.; Schroeder, L.; Donnini, S.; Lehtivuori, H.; Isaksson, L.;
10
11 Thöing, C.; Modi, V.; Berntsson, O.; Stucki-Buchli, B.; Liukkonen, A. Chromophore–
12
13 Protein Interplay During the Phytochrome Photocycle Revealed by Step-Scan FTIR
14
15 Spectroscopy. *Journal of the American Chemical Society*. **2018**, *140*, 12396-404.
16
17
18
19 85. DeLano, W. L. The PyMOL Molecular Graphics System, Version 2.0.6 Schrödinger,
20
21 LLC. **2002** (<https://pymol.org/2/>).
22
23
24
25
26
27
28
29
30
31
32
33
34
35
36
37
38
39
40
41
42
43
44
45
46
47
48
49
50
51
52
53
54
55
56
57
58
59
60

TABLE OF CONTENTS GRAPHIC

